ADVANCED NANOBIOMED RESEARCH Open Access
www.advnanobiomedres.com

Enhanced Exosome Production in Mesenchymal Stem Cells via Extracellular Matrix-Incorporated 3D Spheroid Printing

*Jun-Ho Heo, Min Kyeong Kim, Sang Jin Lee, and Hyun-Wook Kang**

Mesenchymal stem cell (MSC)-derived exosomes (MSC-exosomes) are emerging as promising cell-free therapeutic agents that address many challenges associated with traditional cell-based therapies. However, conventional methods for isolating MSC-exosomes using 2D culture systems are often limited in their efficiency, posing challenges to large-scale production. This study introduces a novel approach to boost MSC-exosome production by promoting cell–cell and cell–extracellular matrix (ECM) interactions. Specifically, ECM-integrated MSC spheroid bioprinting technology is employed to optimize exosome secretion, analyzing the effects of spheroid size and ECM composition on exosome production. It is demonstrated that smaller spheroids constructed using MSCs exhibit an enhanced production of exosomes. Additionally, incorporating ECM components, such as fibrin, Matrigel, and collagen, particularly at higher concentrations, further boosts exosome production. Among these, MSC spheroids with a 150 μm diameter and 0.6% w/v collagen integration demonstrate the highest exosome secretion, achieving an 18.4-fold increase compared to traditional 2D culture systems. Furthermore, exosomes derived from ECM-enhanced MSC spheroids exhibit strong efficacy in an in vitro scratch wound assay, underscoring their therapeutic potential. Thus, the newly developed ECM-incorporated spheroid bioprinting technology offers a highly effective strategy for scaling up MSC-exosome production, paving the way for exosome-based therapeutic applications.

1. Introduction

Mesenchymal stem cells (MSCs) have shown marked potential in cell therapies for treating various diseases due to their regenerative characteristics and have been widely utilized in clinical trials.[1] However, MSC-based therapy still faces several unresolved challenges, including immunogenicity, tumorigenicity, and ectopic tissue formation.[2] Since MSC-based therapies depend on the use of live cells, they inherently face challenges in precisely regulating cellular behavior after transplantation. Consequently, there is a growing demand for therapeutic strategies that can retain the advantages of cell-based therapies while minimizing the risks associated with the unpredictable nature of live cells. In this regard, extracellular vesicles (EVs)—key mediators of MSC paracrine effects—are emerging as a compelling alternative to direct MSC transplantation. Recent studies have highlighted MSC-derived exosomes (MSC-exosomes) as key factors in MSC therapy, drawing considerable attention as a cell-free therapy. Exosomes are a subclass of EVs with diameters ranging from ≈50 to 150 nm. They are structurally composed of a phospholipid bilayer membrane and are secreted by nearly all cell types.[3] Exosomes contain bioactive components, such as mRNA, microRNA, proteins, and amino acids, which enable them to regulate intercellular metabolism and activate various signaling pathways through paracrine effects.[4] Notably, exosomes play a critical role in maintaining normal cellular functions and act as key regulators of disease development and progression.

Recent studies have demonstrated the therapeutic efficacy of MSC-exosomes in tissue regeneration.[5] For instance, MSC-exosomes have shown renoprotective effects in acute kidney injury via anti-inflammatory, immunomodulatory, antinecroptosis, and antiapoptotic mechanisms.[6] Furthermore, in chronic liver diseases, such as liver fibrosis, MSC-exosomes modulate M2 macrophages and contain factors with immunoregulatory roles, such as PGE-2, contributing to the alleviation of disease conditions.[7] However, the clinical application of exosome-based therapies remains limited, primarily because of the low exosome production efficiency.[8] A sufficient supply of exosomes is essential to achieve therapeutic efficacy in clinical applications by effectively mediating intercellular communication and regulation. 2D culture plates, which are a commonly used cell culture method, have limitations in effectively producing exosomes. In particular, the exosome yield per cell is limited in 2D cultures, often necessitating the collection of liters of conditioned medium (CM) to

J.-H. Heo, M. K. Kim, H.-W. Kang
Department of Biomedical Engineering
Ulsan National Institute of Science and Technology
50, UNIST-gil, Ulju-gun, Ulsan 44919, South Korea
E-mail: hkang@unist.ac.kr

J.-H. Heo, S. J. Lee
Wake Forest Institute for Regenerative Medicine
Wake Forest University School of Medicine
Winston-Salem, NC 27157, USA

The ORCID identification number(s) for the author(s) of this article can be found under https://doi.org/10.1002/anbr.202500007.

DOI: 10.1002/anbr.202500007

obtain a clinically relevant quantity of exosomes.[9] This limitation is regarded as a key barrier for the large-scale production of exosome-based therapeutics.[10] Therefore, the development of novel culture methods to improve exosome production efficiency is necessary.

3D culture methods, such as cell spheroids, can be utilized to enhance exosome production efficiency.[11] For example, methods to increase exosome production by mass culturing MSCs in 3D using bioreactors have been investigated.[12] In addition, Kim et al. demonstrated that inducing 3D MSC spheroid formation through the hanging drop method or nonadherent surface coating resulted in higher exosome yields than in 2D cultures.[13] However, conventional cell spheroids often form simple cell clusters without considering the presence of proper extracellular matrix (ECM). The ECM plays a critical role in recapitulating the in vivo environment, which is essential for maintaining and enhancing MSC functionalities, such as stemness and multipotency.[14] While several studies have employed micropatterned or micromold systems to incorporate ECM components during spheroid formation.[15] For instance, Zhu et al. induced cell aggregation by seeding cells onto micropatterned ECM-coated substrates. In contrast, Gonzalez-Fernandez et al. fabricated cell spheroids by directly pipetting a mixture of cells and ECM components into micromolds. Notably, 3D bioprinting technology has emerged as a promising approach for the precise and controllable fabrication of ECM-incorporated spheroids.[16] However, studies on fabricating spheroids that consider ECM components specifically designed to optimize exosome production are still limited. Therefore, there is a need to develop a novel MSC culture platform with ECM-incorporated spheroids, ultimately aiming to enhance exosome yield and facilitate clinical translation.

In this study, we utilized human placenta-derived stem cells (PSCs) as a source of exosomes for therapeutic applications. Previously, we evaluated the capacity of PSC-derived EVs to induce cellular differentiation in vitro, comparing their performance to that of EVs derived from well-characterized bone marrow-derived MSCs (BMSCs).[17] Our findings demonstrated the feasibility of using PSC-derived EVs for bone tissue engineering. Results showed that PSCs proliferate at a significantly faster rate than BMSCs and produce EVs with greater potency. These advantages position PSCs as a promising alternative to BMSCs for applications requiring large quantities of EVs or enhanced therapeutic efficacy. Building on these insights, we further aimed to enhance the therapeutic potential and production efficiency of exosomes by developing ECM-incorporated spheroids using 3D bioprinting technology. This approach was designed to simultaneously enhance cell–cell and cell–ECM interactions. This spheroid printing method enables precise control over the morphology and biochemical properties of PSC spheroids by adjusting the process parameters and bioink composition. To optimize the exosome extraction process, we first analyzed the effect of the spheroid diameter on exosome productivity. Subsequently, we investigated the composition and concentration of the ECM incorporated into PSC spheroids and analyzed their impact on the characteristics and quantity of isolated exosomes. Finally, we evaluated the therapeutic efficacy of ECM-incorporated PSC spheroid-derived exosomes by assessing their in vitro wound healing functionality. The results demonstrate that exosomes derived from ECM-incorporated PSC spheroids offer enhanced production efficiency and hold significant potential for application in exosome-based therapeutics and clinical research.

2. Results

2.1. Isolation of ECM-Incorporated MSC Spheroid-Derived Exosomes

To enhance the MSC-exosome production yield, we developed an ECM-incorporated MSC spheroid printing technology (**Figure 1**A). To fabricate ECM-incorporated spheroids, a poly(ε-caprolactone) (PCL) frame was first printed, followed by the deposition of a cell-free alginate-based bioink. MSC-laden, ECM-based bioinks were then printed into this alginate layer. After crosslinking to form alginate matrix and subsequent culture, noncrosslinked and soluble components such as gelatin and hyaluronic acid gradually diffused out, creating voids within the matrix (Figure S1, Supporting Information). Because of the noncell-adhesive nature of the alginate matrix, the printed cells aggregated within these voids and formed spheroids. During this aggregation process, ECM components distributed among the cells were incorporated into the spheroids, resulting in the formation of ECM-incorporated spheroids. Consequently, early cell–ECM interactions were induced within these ECM-incorporated MSC spheroids. The in vivo relevant microenvironment created through the simultaneous consideration of cell–cell and cell–ECM interactions enhanced the therapeutic exosome secretion of MSC spheroids (Figure 1B). Figure 1C illustrates the process of exosome extraction from the printed spheroids. The CM was collected, and secreted MSC-exosomes were isolated in pellet form using a precipitation-based method.

2.2. Effect of the Size of Printed Spheroid on Exosome Production

To evaluate the effects of the printing process and spheroid size on exosome production, MSC spheroids with diameters ranging from 150 to 250 μm were fabricated using the bioprinting method. **Figure 2**A presents a still image of the MSC spheroid printing process, demonstrating the precise patterning of the PSC-laden bioink into spherical shapes within the PCL frame and an alginate-based matrix using a needle nozzle. Microscopic observations revealed that the cells were dispersed right after the printing process. However, by day 1, the cells began to form spheroid structures with smooth surfaces. Live/dead staining on days 1 and 3 showed that most PSCs stained green, indicating high cell viability (Figure 2B). This confirmed that the developed printing process did not adversely affect the viability of the PSCs. In addition, bright-field images taken on day 3 confirmed that spheroids with diameters ranging from 150 to 250 μm maintained their printed sizes (Figure 2C). Next, the morphological characteristics of the printed spheroids were analyzed (Figure 2D,E). Regardless of spheroid diameter, all samples exhibited aspect ratios below 1.2 and roundness values above 0.8. These findings demonstrate that uniformly shaped, spherical spheroids with diameters ranging from 150 to 250 μm can be consistently fabricated by optimizing the printing dispensing

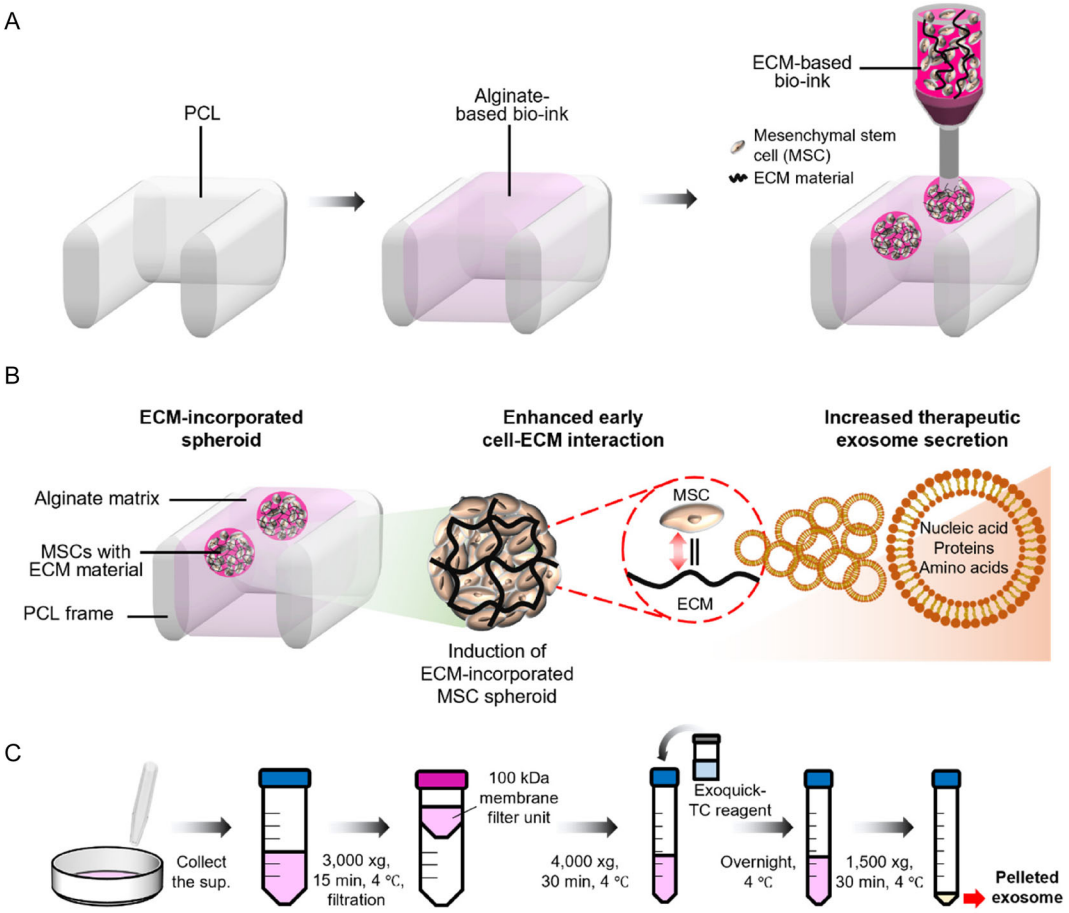

Figure 1. Schematic illustration of ECM-incorporated spheroid printing process and exosome isolation procedure. A) Schematic illustration of ECM-incorporated spheroid printing process. B) Formation of ECM-incorporated MSC spheroids with enhanced early cell–ECM interactions and elevated exosome production. C) Schematic overview of exosome isolation from conditioned media.

parameters. Furthermore, the live/dead staining images for each spheroid size on day 3 demonstrated consistently high cell viability across all groups (Figure 2F). To further assess the impact of spheroid size on exosome production, we quantified the amount of isolated exosomes from spheroids with varying diameters. ATP levels measured from each size group were used to normalize exosome yields, serving as an indicator of viable cell numbers. As spheroid diameter increased, ATP levels increased accordingly, suggesting a higher number of viable cells in larger spheroids (Figure 2G). When exosome yield was normalized to ATP content, smaller spheroids demonstrated greater exosome production efficiency (Figure 2H). Notably, spheroids with a diameter of 150 μm exhibited ≈2.6-fold higher exosome production efficacy compared to spheroids with diameters of 200 and 250 μm.

2.3. Characterization of Exosomes Derived from 3D Printed Spheroids

To evaluate the effects of the spheroid printing process on exosome productivity and characteristics, we compared exosomes derived from the spheroid printing group with those from the 2D and conventional mold groups prepared using ultralow attachment U-shaped microwells (**Figure 3**A). A comparison of the exosomal protein yields isolated from each group revealed that the spheroid printing group exhibited ≈5.5- and 2.7-fold higher exosome productivity than the 2D and conventional mold groups, respectively (Figure 3B). Next, we analyzed the morphology and size of exosomes isolated from each group. Transmission electron microscopy (TEM) imaging confirmed the presence of a lipid bilayer structure in the exosomes from all groups (Figure 3C). Additionally, dynamic light scattering (DLS) measurements showed that the average diameters of the exosomes across all groups ranged from 91.3 to 110.8 nm, with no significant differences observed (Figure 3D). The isolated exosomes were further characterized by Western blot analysis of exosome-specific protein markers (Figure S2, Supporting Information). The membrane-associated marker CD9 and the endosome-related marker TSG101 were both detected, confirming the presence of typical exosomal proteins. These results indicate that exosomes produced via the 3D spheroid printing technique retain typical structural features and marker expression comparable to those derived from conventional culture methods, while exhibiting enhanced production efficiency.

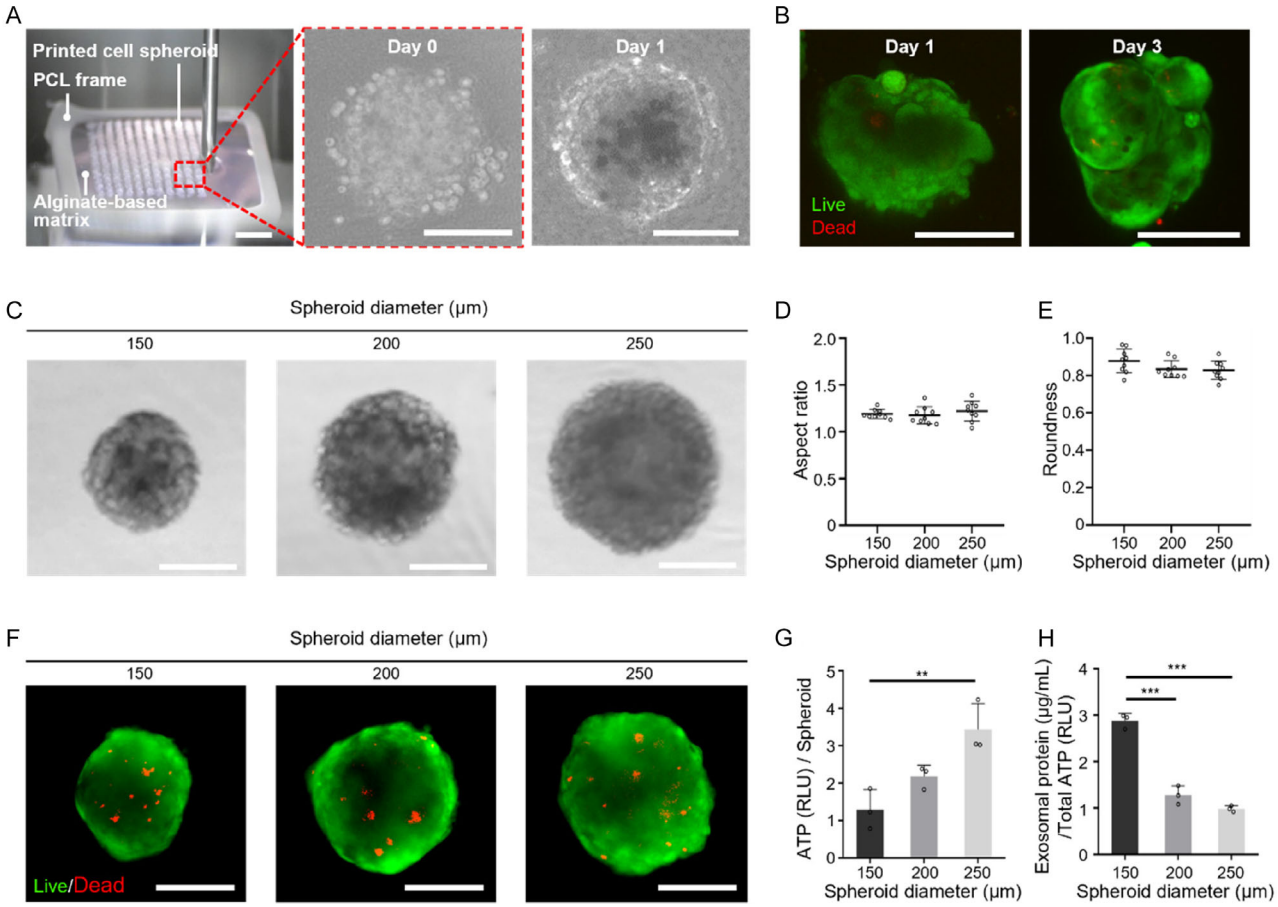

Figure 2. Characterization of various sizes of printed PSC spheroids. A) Still image (left panel) of the spheroid printing process with PCL frame, alginate-based matrix and PSC-laden bioink, and bright-field images (middle and right panels) of PSC spheroids right after printing and on day 1, respectively (scale bars: 2 mm for still image and 100 μm for bright-field images, respectively). B) Representative live (green) and dead (red) staining images of PSC spheroid on day 1 after printing (scale bars: 100 μm). C) Bright-field images of PSC spheroids with diameters ranging from 150 to 250 μm on day 3 (scale bars: 100 μm). Aspect ratio D) and roundness E) of printed spheroids with diameters ranging from 150 to 250 μm, calculated from bright-field images. F) Representative fluorescence images of live (green) and dead (red) staining results depending on the spheroid sizes 3 days after printing (scale bars: 100 μm). G) ATP content of spheroids with diameters ranging from 150 to 250 μm, fabricated by adjusting the dispensing time. H) Extracted exosomal protein concentration according to the sizes of spheroid. The total protein contents of exosomes were normalized with total viable cells. All data are expressed as mean ± SD (***$P < 0.001$; ns, not significant).

2.4. Effect of ECM Incorporation on Exosome Secretion in Printed MSC Spheroids

The effects of the ECM components in the printed MSC spheroids on exosome characteristics were evaluated. Spheroids incorporating fibrin, Matrigel, or collagen were printed at 0.1–0.6% w/v concentrations (**Figure 4**A). Viability assessment of ECM-incorporated spheroids demonstrated a high cell survival rate, indicating that the ECM-incorporated spheroid printing process is cytocompatible (Figure S3, Supporting Information). Exosomal protein yield was measured, and the results were compared with those obtained from the conventional mold group (Figure 4B–D). The results indicated that the amount of exosomal proteins increased with higher ECM concentrations across all ECM groups. Notably, at a concentration of 0.6% w/v, all ECM groups exhibited a dramatic enhancement in exosome production efficacy. Compared to spheroids produced using the conventional mold, exosome production in printed spheroids incorporated with 0.6% w/v fibrin, Matrigel, and collagen increased by ≈5.9-fold, 8.4-fold, and 9.1-fold, respectively. To evaluate the potential effect of biomaterials on protein content in the CM, cell-free constructs were printed using the bioinks and analyzed using a BCA assay. Only minimal protein levels were detected, confirming that residual biomaterials in the bioinks have a negligible impact on the exosome isolation process (Figure S4, Supporting Information). TEM analysis of exosomes isolated from each group revealed the presence of a lipid bilayer structure, a characteristic feature of exosomes, in all groups (Figure 4E). To analyze the average size of exosomes derived from the different ECM-incorporated spheroids, DLS analysis was conducted. The results showed that the average sizes of exosomes from fibrin, Matrigel, and collagen groups were 99.44 ± 39.83, 113.9 ± 45.20, and 93.11 ± 35.47 nm, respectively.

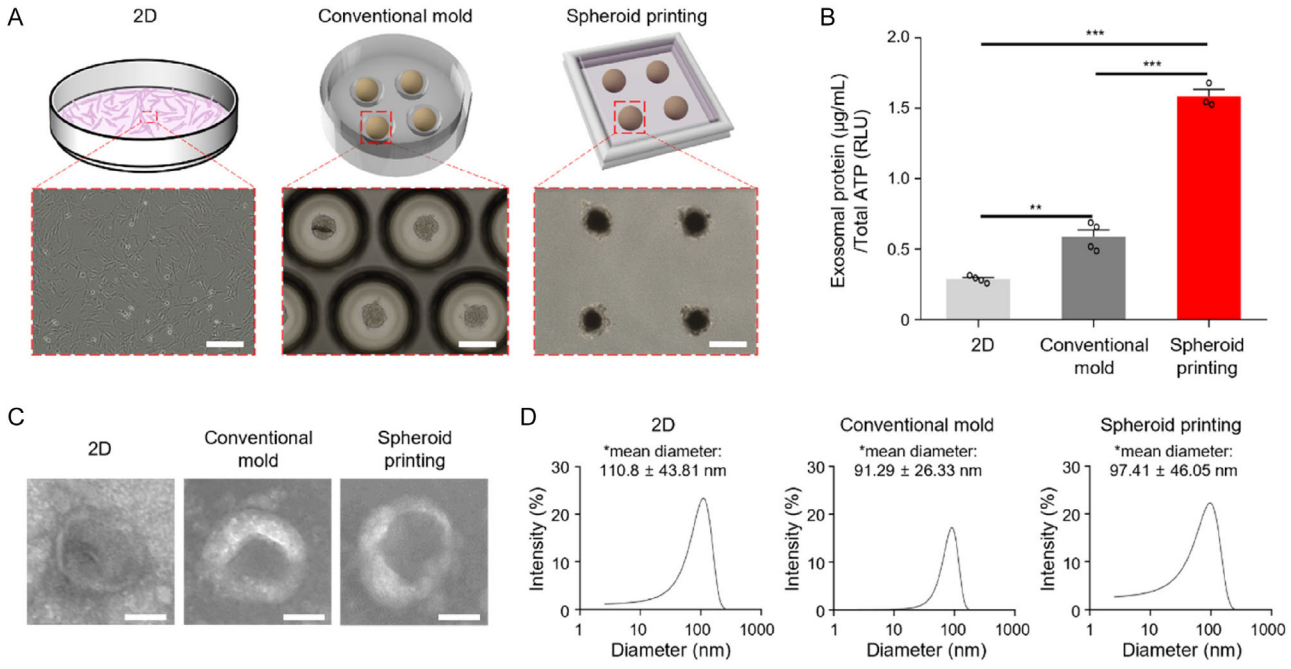

Figure 3. Effect of 3D spheroid printing on the exosome productivity from PSCs. A) Schematic representation of the experimental groups. PSCs were cultured in a cell culture dish (2D) or in an ultra-low attachment U-shaped microwell (conventional mold) or printed within alginate-based bioink (Spheroid printing) (scale bars: 100 μm). B) Productivity of exosomes derived from each group. The total protein contents of exosomes were normalized with total viable cells for each group. C) TEM images of exosome isolated from each group (scale bars: 50 nm). D) DLS analysis data of exosome isolated from each group. All data are expressed as mean ± SD (*$P < 0.05$; **$P < 0.01$; ***$P < 0.001$).

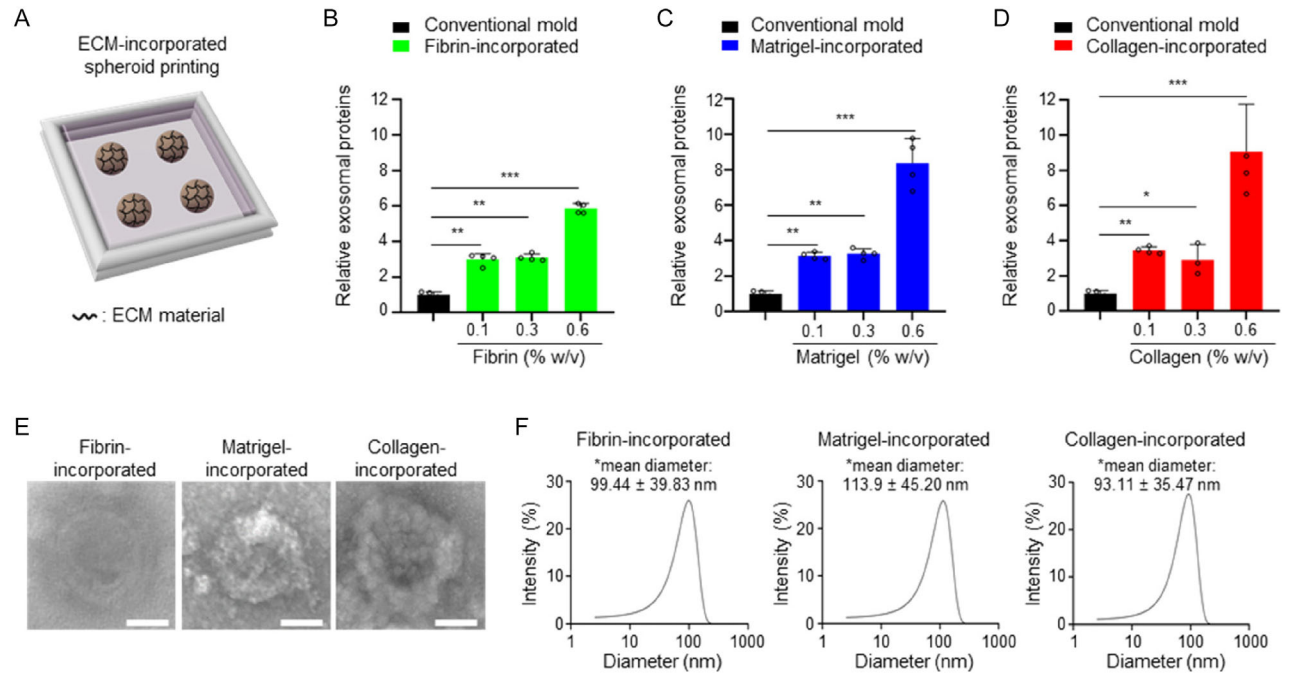

Figure 4. Effect of ECM incorporation on exosome productivity from PSCs. A) Schematic representation showing the PSC spheroid incorporated with ECM material. Productivity of exosomes derived from B) fibrin-, C) Matrigel-, and D) collagen-incorporated spheroid. The total protein contents of exosome were normalized with total viable cells and was expressed as fold change based on the conventional mold group. E) Representative TEM images of exosomes isolated from each group (scale bars, 50 nm). F) DLS analysis data of exosomes isolated from each group. All data are expressed as mean ± SD (*$P < 0.05$; **$P < 0.01$; ***$P < 0.001$).

These results confirm that the size distribution of exosomes was uniform, regardless of the type of ECM incorporated (Figure 4F). These findings demonstrated that ECM incorporation significantly enhanced exosome production in MSC spheroids. Based on these experimental results, the 0.6% w/v collagen-incorporated spheroid group which exhibited the highest exosome yield was selected for subsequent experiments.

2.5. Wound Healing Effect of Exosomes Derived from Collagen-Incorporated MSC Spheroids

A scratch wound assay was performed to evaluate the wound healing efficacy of the isolated exosomes. After treating human dermal fibroblasts (hDFs) monolayers with exosomes for 8 h, bright-field imaging revealed that the exosome-treated groups exhibited enhanced wound closure through cell migration (**Figure 5**A). Quantitative wound closure data based on bright-field images showed that the wound healing ability increased significantly and dose-dependently with higher exosome concentrations (Figure 5B). Notably, the collagen-incorporated spheroid-derived exosome group demonstrated a significant wound closure effect at a low concentration of 10 μg mL^{-1} (54.4 ± 2.7%), compared with the depleted medium group (38.1 ± 6.6%). At a high exosome concentration of 100 μg mL^{-1}, both the conventional mold group and the collagen-incorporated spheroid group exhibited high wound healing efficacy, achieving 76.5 ± 4.7% and 78.4 ± 3.8% wound closure, respectively.

3. Discussion

In this study, MSC-exosome production was significantly enhanced using ECM-incorporated spheroid printing. MSC-exosomes have shown therapeutic effects in various tissue damage models, including angiogenesis, osteogenesis, and wound closure.[18] However, traditional 2D cell culture methods result in low exosome production yields, which limit the efficiency and clinical applicability of exosome-based therapies.[19] Therefore, addressing these time-consuming and inefficient issues is critical for clinical applications. To overcome these limitations, we utilized an ECM-incorporated spheroid-printing technology that significantly increased the exosome yield (Figure 1A). Unlike traditional spheroid culture methods that primarily focus on cell–cell interactions, ECM-incorporated spheroids facilitate the integration of both cell–cell and cell–ECM interactions within the spheroid.[20] Our previous studies demonstrated that ECM-incorporated spheroids, which consider both cell–cell and cell–ECM interactions, improve hepatic functionality of primary hepatocytes compared to spheroids where ECM materials are not incorporated.[21]

Our experimental results revealed that the spheroid size significantly affected exosome production. After printing spheroids of various diameters and comparing their exosome yields, we found that smaller spheroids yielded higher amounts of exosomes (Figure 2C,D). It is known that the diameter of the cell spheroid affects functionality of cell spheroids.[22] Especially, Kim et al. demonstrated that smaller spheroids created using conventional hanging drop or nonadherent coating methods resulted in more efficient exosome production.[13] These findings highlight the importance of optimizing the spheroid size to maximize exosome production efficiency.

The 3D culture method provides an environment similar to in vivo, enhancing cell proliferation and increasing exosome secretion. In particular, for MSCs, it helps maintain stemness and improve the paracrine effect.[13,23] When MSCs are cultured in a nonadherent environment to form spheroids, the decreased expression of F-actin creates a favorable environment for exosome production and secretion.[13] Additionally, the mildly hypoxic environment in the center of spheroids formed during culture enhances exosome production.[24] The developed spheroid printing group, a type of 3D culture method, showed a significantly increased exosome production yield compared to the 2D group (Figure 3B). Furthermore, our spheroid printing method was shown to improve exosome production compared to conventional spheroid fabrication methods. Traditional spheroid fabrication methods typically use hanging drop or nonadherent coating methods, in which ECM materials are not properly considered. In this study, bioinks made from

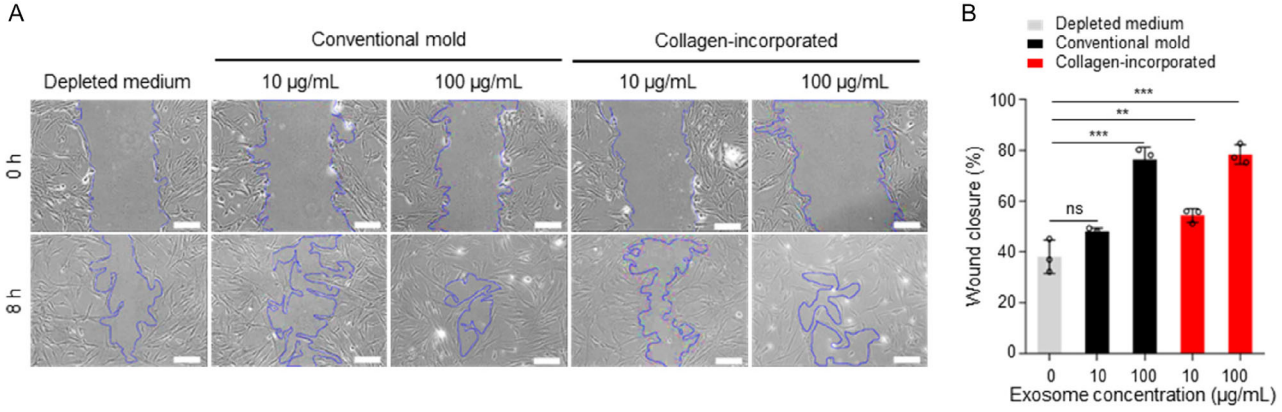

Figure 5. Investigation of wound healing ability of PSC-derived exosomes using scratch assay. A) Bright-field images of the wounded hDF monolayer at 0 and 8 h after treatment with depleted medium, or exosomes (10 or 100 μg mL^{-1}) derived from conventional mold spheroids or collagen-incorporated spheroids. Blue line indicates the edge of the wound (scale bars, 200 μm). B) Percentage of wound closure 8 h after treatment with various concentrations of exosomes. All data are expressed as mean ± SD (**$P < 0.01$; ***$P < 0.001$; ns, not significant).

various cytocompatible biomaterials were used to fabricate spheroids. Among the bioink components, gelatin and hyaluronic acid are known to support MSC proliferation and functionality.[25] Additionally, the biomechanical cues of the bioink used in the spheroid printing process likely contributed to increased exosome production. When MSCs are cultured on surfaces with lower stiffness, the secretion of various factors increases compared to those cultured on tissue culture plates or surfaces with higher stiffness.[26] In this study, the printed MSC spheroids were encapsulated within an alginate matrix, which exhibits lower stiffness compared to conventional plastic culture surfaces or agarose molds commonly used for spheroid formation.[27] This softer microenvironment may have contributed to enhanced exosome secretion. Therefore, the biochemical and biomechanical properties of the bioink likely contributed to the increased exosome production in printed spheroids compared with conventional spheroid formation methods.

The exosome production yield can be significantly increased through ECM incorporation.[28] The incorporation of fibrin, Matrigel, and collagen into the printed MSC spheroids enhanced exosome production in an ECM concentration-dependent manner (Figure 4B–D). This increase in ECM content is presumed to have supported improved MSC viability and functionality by promoting enhanced cell–ECM interactions within the spheroids. Notably, the spheroids containing 0.6% w/v collagen showed approximately a 9.1-fold increase in exosome production compared to conventional mold group. In a previous study, we confirmed that, in ECM-incorporated spheroids, a thin ECM layer was formed between the cells constituting the spheroid.[21] Unlike conventional spheroid formation, which primarily enhances cell–cell interactions, ECM incorporation also facilitates early cell–ECM interactions within the spheroid. As a result, spheroids fabricated using the ECM-incorporated printing technique exhibit both enhanced cell–cell and cell–ECM interactions, which collectively contribute to significantly increased exosome production compared to spheroids formed by 2D or conventional methods.

Dermal fibroblasts play a key role in ECM remodeling and wound contraction during wound healing. In chronic wound models, the functions of fibroblasts, including migration, proliferation, and growth factor secretion, are diminished.[29] According to Shabbir et al. MSC-derived exosomes influence wound healing signaling pathways such as STAT3 in fibroblasts, promoting migration and demonstrating wound healing effects.[30] Exosomes derived from ECM-incorporated spheroids created in this study also exhibited therapeutic effects in an in vitro wound healing assay. Notably, even at a low concentration (10 $\mu g\,mL^{-1}$), exosomes from ECM-incorporated spheroids showed improved wound closure compared to those from conventional molds, and at a high concentration (100 $\mu g\,mL^{-1}$), around 80% wound closure was observed (Figure 5). These data showed that the incorporation of the ECM into spheroids can enhance their therapeutic efficacy. Therefore, exosomes extracted from ECM-incorporated spheroids are likely to contain components that influence fibroblast migration signaling pathways, contributing to effective results in the scratch wound assay. Zhang et al. also demonstrated that when BMSCs are cultured on collagen scaffolds, not only is exosome production increased but their therapeutic effects are also enhanced.[31] However, further research is required to analyze the different profiles of proteins and genetic material present in the exosomes from printed spheroid group.

This study demonstrates that ECM-incorporated spheroid printing technology can significantly enhance MSC-derived exosome production. Notably, exosomes extracted using this method also exhibited excellent therapeutic effects, making a substantial contribution to the large-scale production of exosome-based therapeutics and greatly expanding their clinical applicability. In future studies, exosomes derived from spheroids incorporating various cell types and tailored ECM materials will be extracted and effectively utilized in cell-free therapies for disease treatment.

4. Conclusion

In this study, we developed a novel ECM-incorporated MSC spheroid that significantly enhanced exosome production by simultaneously considering cell–cell and cell–ECM interactions. Using 3D bioprinting technology, we were able to precisely control the diameter and biochemical properties of MSC spheroids by adjusting the printing process and bioink composition. Using this precise control technology, we compared and analyzed exosome production yields based on spheroid size and the type and concentration of incorporated biomaterials. The collagen-incorporated MSC spheroids, with an optimized size of ≈150 μm in diameter, exhibited an 18.4-fold increase in exosome production compared to 2D culture methods. Furthermore, exosomes extracted from the fabricated spheroids showed excellent wound-healing effects in a scratch wound assay using hDF. The ECM-incorporated MSC spheroids produced in this study are expected to enhance the exosome production efficiency, thereby increasing the potential for the clinical application of exosome-based therapies.

5. Experimental Section

Cell Culture: To print the MSC spheroids, human PSCs were used for this study. Human PSCs were obtained and isolated from healthy donors with informed consent approved according to the procedures of the Institutional Review Board (IRB, # 00 056 941) at Wake Forest University (Winston-Salem, NC), and cells from passage 5 to 7 were cultured in Dulbecco's Modified Eagle's Medium (DMEM, Gibco, USA), 10% v/v fetal bovine serum (FBS, ScienCell, USA), 100 U mL^{-1} penicillin G, and 100 μg mL^{-1} streptomycin (Gibco) at 37 °C in an incubator with 5% CO_2 atmosphere and 100% relative humidity. hDFs were purchased from ATCC cultured in DMEM high glucose supplemented with 10% v/v of FBS (Gibco) and 100 U mL^{-1} penicillin G, and 100 μg mL^{-1} streptomycin and cells from passages between 5 and 7 were used. For the 2D culture group, PSCs were cultured in 225 cm^2 cell culture flasks (Corning, USA). For the conventional spheroid group, PSCs were seeded in Elplasia 6-well black round-bottom ultralow attachment plates (Corning).

Preparation of Bioinks: Five types of bioinks were prepared for this study: alginate-, gelatin-, fibrin-, Matrigel-, and collagen-based bioinks. First, hyaluronic acid (HA; Sigma, USA) was dissolved in Minimum Essential Medium (ATCC, USA) at 37 °C overnight under gentle rotation. Following complete dissolution, gelatin (Sigma) and sodium alginate (Sigma) were added to formulate the alginate-based bioink. For the preparation of gelatin-based and ECM-based bioinks, gelatin, $CaCl_2$ (Junsei Chemical Co., Japan), fibrinogen (Sigma), Matrigel (Corning), and collagen (Corning) were similarly dissolved in the HA solution under the same

conditions. The specific concentrations of each component in the respective bioinks are provided in Table S1 (Supporting Information). All bioinks were sterilized using a 0.45 μm filter and stored at –80 °C until use.

3D Printing of MSC Spheroids: To print the spheroids, a previously developed biodot printing process was performed.[26] Briefly, PCL as a structural frame was printed through a 300 μm dispensing nozzle (ARQUE, TECDIA, Republic of Korea) at 90 °C, 200 kPa, and 150 mm min^{-1} printing speed. The soft matrix part composed of alginate-based bioink was printed with 600 μm height, 0.221 μL s^{-1} dispensing rate, and 50 mm min^{-1} printing speed, through a 300 μm dispensing nozzle (ARQUE, TECDIA). For cell printing, 7×10^8 cells mL^{-1} of PSCs were homogeneously mixed with gelatin-, fibrin-, Matrigel-, or collagen-based bioink and loaded into a syringe. The gelatin-based bioink, which lacked fibrin, Matrigel, and collagen, was used to print spheroids without ECM incorporation and served as the control group. The cell-laden bioinks were printed into a dot shape through a needle nozzle with an inner diameter of 120 μm at a 0.0069 μL s^{-1} dispensing rate. To achieve various size such as 150, 200, and 250 μm diameter of printed spheroids, dispensing time of 2, 5, and 8 s was applied, respectively. Following printing, the constructs were crosslinked at 37 °C for 30 min using a 40 mM $CaCl_2$ solution containing 2.5 U mL^{-1} thrombin. During this process, alginate was ionically crosslinked by $CaCl_2$, fibrinogen was enzymatically crosslinked by thrombin, and both collagen and Matrigel underwent thermal gelation. The crosslinked constructs were subsequently cultured at 37 °C in a CO_2 incubator, allowing for the gradual dissolution of noncrosslinked and soluble sacrificial components.

Characterization of the Bioprinted Cell Spheroid: Bright-field images of the printed cell spheroids were captured using a microscope (Leica, Germany). Morphological characteristics were analyzed using ImageJ software (NIH, USA). The aspect ratio was determined by dividing the major axis length by the minor axis length of each spheroid. Roundness was calculated using the following equation:

$$\text{Roundness} = \frac{4 \times \text{Area}}{\pi \times \text{Major axis}^2}$$

MSC Spheroid Viability Test: The viability of PSC spheroids was analyzed using a LIVE/DEAD viability kit (Invitrogen, USA). The fabricated PSC spheroids were washed with Dulbecco's phosphate-buffered saline (DPBS) and incubated with 0.5 μL mL^{-1} of Calcein AM and 2 μL mL^{-1} of Ethidium homodimer-1 in DPBS. After incubation, fluorescence images were obtained using an Olympus Fluoroview Fv10i laser confocal microscope (Olympus, Tokyo, Japan). For quantification, ImageJ software (NIH, Bethesda, MD, USA) was used with triplicate images to calculate viable cell percentages.

Isolation of Exosomes: For exosome isolation, 2D-cultured PSCs and PSC spheroids were initially cultured in growth medium for 3 days. During this period, spheroid formation occurred in the printed groups, accompanied by the gradual diffusion of uncrosslinked biomaterials. The medium was then replaced with serum-depleted MEM (Gibco), and the cultures were maintained for an additional three days. After 3 days, the CM containing exosomes secreted by either 2D-cultured cells or cell spheroids was collected and centrifuged at 3 000 g for 15 min at 4 °C to eliminate dead cells and cellular debris. Then, the supernatant was transferred to the 0.2 μm syringe filter unit (Sartorius, Germany), followed by centrifuged with 100 kDa membrane filter unit (Merck-Millipore, USA) at 4 000 g for 30 min at 4 °C to concentrate CM and remove unwanted small proteins. The concentrated medium was mixed with ExoQuick-TC (System Biosciences, USA) reagent with volume ratio of 5:1 and incubated overnight at 4 °C. Then, the mixture was centrifuged at 1 500 g for 30 min at 4 °C, and the pelleted exosomes derived from PSCs were resuspended in 100 μL of PBS.

Measurement of the Cell Number and Exosomal Proteins: To compare and normalize the exosome yield among the experimental groups, the concentration of exosomal proteins was normalized to total ATP. To extract exosomal proteins, exosomes were lysed for 30 min in ice-cold radioimmunoprecipitation assay buffer supplemented with a protease inhibitor cocktail (Thermo Scientific, USA), followed by vortex mixing. The lysed samples were centrifuged at 12 000 rpm for 10 min at 4 °C to harvest proteins. The concentrations of exosomal proteins were measured by Pierce Bicinchoninic acid (BCA) protein assay kit (Thermo Scientific). The total ATP from PSCs in each group was quantified using the CellTiter-Glo 3D Cell Viability Assay (Promega, USA) according to manufacturer's instructions. Since the number of cells in each group could influence the amount of extracted exosomal proteins, exosome quantities measured by the BCA assay were normalized to ATP levels to enable a comparative analysis of exosome yield.

SDS-PAGE and Western Blot Analysis: Isolated exosomal proteins were separated by 10% SDS-PAGE and transferred onto PVDF membranes (Merck-Millipore). After blocking with 5% skim milk in tris-buffered saline with Tween 20, the membranes were incubated overnight at 4 °C with primary antibodies against CD9, TSG101, and β-actin (all from Abcam, UK). The membranes were then incubated with HRP-conjugated secondary antibodies (Abcam) and developed using an enhanced chemiluminescence solution (Invitrogen). Protein bands were visualized using a ChemiDoc imaging system and analyzed with ImageLab software (Bio-Rad, USA).

TEM and DLS Analysis of Exosomes: The morphology and size of exosomes were analyzed using TEM and DLS. For TEM analysis, 100 μg mL^{-1} exosome solution was dried on copper mesh grid. The exosome-loaded copper mesh grid was negatively stained with uranyl acetate (Polysciences) and imaged using TEM (FEI, Tecnai BioTwin 120 kV TEM, Thermo Scientific). To analyze the size distribution of the isolated exosomes, DLS was performed using a particle size analyzer (Brookhaven Instruments Corporation, USA). Each group was analyzed in triplicate, and a Gaussian model was fitted to the particle size distribution to calculate the average diameter.

Scratch Wound Assay: hDFs were seeded in 6 well-plate and cultured until reaching 90% confluency. Wounds were mechanically created by scraping with a 200 μL micropipette tip. Detached cells were washed with PBS and wounded monolayers were treated with different sources and concentrations of intact PSC-derived exosomes (0, 10, or 100 μg mL^{-1}) and tracked through bright-field microimaging. The exosome treatment concentration was determined based on BCA assay results of lysed exosomes obtained from conventional mold-derived and collagen-incorporated spheroid groups.

Statistical Analysis: Data are presented as mean ± standard deviation (SD). Multiple comparisons between experimental groups were conducted using one-way analysis of variance, followed by Tukey's multiple comparison test.

Supporting Information

Supporting Information is available from the Wiley Online Library or from the author.

Acknowledgements

J.H. and M.K.K. contributed equally to this work. The authors thank the Manufacturing Development Center at Wake Forest Institute for Regenerative Medicine for the human PSC isolation. This study was supported by the Institute of Civil Military Technology Cooperation funded by the Defense Acquisition Program Administration and Ministry of Trade, Industry and Energy of the Korean government (No. 22-CM-BR-12) and the Bio&Medical Technology Development Program of the National Research Foundation (NRF) funded by the Korean government (MSIT) (No. RS-2024-00508821).

Conflict of Interest

The authors declare no conflict of interest.

Data Availability Statement

The data that support the findings of this study are available from the corresponding author upon reasonable request.

Keywords

3D spheroid, bioprinting, exosomes, extracellular matrix, mesenchymal stem cells

Received: January 15, 2025
Revised: June 9, 2025
Published online: July 2, 2025

[1] a) Y. Xiao, H. Li, J. Zhang, S. Yang, C. Zhang, Y. Huang, X. Tang, H. Xie, *Nano Res.* **2024**, *17*, 2836–2856; b) L. Xu, S. Wang, X. Sui, Y. Wang, Y. Su, L. Huang, Y. Zhang, Z. Chen, Q. Chen, H. Du, Y. Zhang, L. Yan, *ACS Appl. Mater. Interfaces* **2017**, *9*, 14716–14723; c) A. J. R. Barcena, J. V. D. Perez, M. R. Bernardino, J. A. Damasco, A. Cortes, H. C. Del Mundo, E. M. D. San Valentin, C. Klusman, G. M. Canlas, F. M. Heralde III, R. Avritscher, N. Fowlkes, R. R. Bouchard, J. Cheng, S. Y. Huang, M. P. Melancon, *Adv. Healthcare Mater.* **2023**, *12*, 2300960.

[2] a) S. Flamant, C. Loinard, R. Tamarat, *Environ. Adv.* **2023**, *13*, 100408; b) G. V. Røsland, A. Svendsen, A. Torsvik, E. Sobala, E. McCormack, H. Immervoll, J. Mysliwietz, J.-C. Tonn, R. Goldbrunner, P. E. Lønning, R. Bjerkvig, C. Schichor, *Cancer Res.* **2009**, *69*, 5331–5339; c) M. Breitbach, T. Bostani, W. Roell, Y. Xia, O. Dewald, J. M. Nygren, J. W. Fries, K. Tiemann, H. Bohlen, J. Hescheler, A. Welz, W. Bloch, S. E. W. Jacobsen, B. K. Fleischmann, *Blood, The Journal of the American Society of Hematology* **2007**, *110*, 1362–1369.

[3] J. J. Lai, Z. L. Chau, S. Y. Chen, J. J. Hill, K. V. Korpany, N. W. Liang, L. H. Lin, Y.-H. Lin, J. K. Liu, Y.-C. Liu, R. Lunde, W.-T. Shen, *Adv. Sci.* **2022**, *9*, 2103222.

[4] a) N. Dilsiz, *Transl. Oncol.* **2024**, *50*, 102121; b) L. Urbanelli, A. Magini, S. Buratta, A. Brozzi, K. Sagini, A. Polchi, B. Tancini, C. Emiliani, *Genes.* **2013**, *4*, 152–170.

[5] S. Deng, H. Cao, X. Cui, Y. Fan, Q. Wang, X. Zhang, *Acta Biomater.* **2023**, *171*, 68.

[6] M. Liu, X. Chen, *Appl. Biochem. Biotechnol.* **2024**, *196*, 7954.

[7] a) S. Mardpour, M. H. Ghanian, H. Sadeghi-Abandansari, S. Mardpour, A. Nazari, F. Shekari, H. Baharvand, *ACS Appl. Mater. Interfaces* **2019**, *11*, 37421–37433; b) H. Liu, R. Yang, S. Zhao, F. Zhou, Y. Liu, Z. Zhou, L. Chen, J. Xie, *Bioeng. Transl. Med.* **2023**, *8*, e10467.

[8] W. Pan, H. Chen, A. Wang, F. Wang, X. Zhang, *Life Sci.* **2023**, *319*, 121524.

[9] R. A. Haraszti, R. Miller, M. Stoppato, Y. Y. Sere, A. Coles, M.-C. Didiot, R. Wollacott, E. Sapp, M. L. Dubuke, X. Ki, S. A. Shaffer, M. DiFiglia, Y. Wang, N. Aronin, A. Khvorova, *Mol. Ther.* **2018**, *26*, 2838.

[10] K. Zhang, K. Cheng, *Nat. Rev. Bioeng.* **2023**, *1*, 608.

[11] a) F. N. Faruqu, R. Liam-Or, S. Zhou, R. Nip, K. T. Al-Jamal, *FASEB J.* **2021**, *35*, e21206. b) W. Yu, S. Li, X. Guan, N. Zhang, X. Xie, K. Zhang, Y. Bai, *Biomater. Adv.* **2022**, *133*, 112646.

[12] D. B. Patel, C. R. Luthers, M. J. Lerman, J. P. Fisher, S. M. Jay, *Acta Biomater.* **2019**, *95*, 236.

[13] M. Kim, H.-W. Yun, D. Y. Park, B. H. Choi, B.-H. Min, *Tissue Eng. Regener. Med.* **2018**, *15*, 427.

[14] F. M. Watt, W. T. Huck, *Nat. Rev. Mol. Cell Biol.* **2013**, *14*, 467.

[15] a) X. Zhu, Q. Wu, Y. He, M. Gao, Y. Li, W. Peng, S. Li, Y. Liu, R. Zhang, J. Bao, *ACS omega* **2022**, *7*, 2364–2376; b) T. Gonzalez-Fernandez, A. J. Tenorio, *Adv. Healthcare Mater.* **2022**, *11*, 2102337.

[16] H.-Y. Lee, J. W. Lee, *J. Funct. Biomater.* **2024**, *15*, 345.

[17] E. Pishavar, J. S. Copus, A. Atala, S. J. Lee, *Tissue Eng., Part A* **2021**, *27*, 1044.

[18] a) P. Gondaliya, A. A. Sayyed, P. Bhat, M. Mali, N. Arya, A. Khairnar, K. Kalia, *Mol. Pharmaceutics* **2022**, *19*, 1294–1308; b) J. Liu, Z. Yan, F. Yang, Y. Huang, Y. Yu, L. Zhou, Z. Sun, D. Cui, Y. Yan, *Stem Cell Rev. Rep.* **2021**, *17*, 305–317; c) N. Al-Sharabi, S. Mohamed-Ahmed, S. Shanbhag, C. Kampleitner, R. Elnour, S. Yamada, N. Rana, E. Birkeland, S. Tangl, R. Gruber, K. Mustafa, *Stem Cell Res. Ther.* **2024**, *15*, 33.

[19] a) S. Thippabhotla, C. Zhong, M. He, *Sci. Rep.* **2019**, *9*, 13012; b) C. He, S. Zheng, Y. Luo, B. Wang, *Theranostics* **2018**, *8*, 237.

[20] M. Yamada, A. Hori, S. Sugaya, Y. Yajima, R. Utoh, M. Yamato, M. Seki, *Lab Chip* **2015**, *15*, 3941.

[21] M. K. Kim, W. Jeong, S. Jeon, H.-W. Kang, *Frontiers in Bioengineering and Biotechnology* **2023**, *11*, 1305023.

[22] L. Cui, Y. Luo, H. Wang, Q. Chen, X. Zhou, Y. Guan, Y. Zhang, *Adv. Mater. Interfaces* **2022**, *9*, 2102327.

[23] a) H. M. Wobma, D. Liu, G. Vunjak-Novakovic, *ACS Biomater. Sci. Eng.* **2017**, *4*, 1162–1175; b) J. Cao, B. Wang, T. Tang, L. Lv, Z. Ding, Z. Li, R. Hu, Q. Wei, A. Shen, Y. Fu, B. Liu, *Stem Cell Res. Ther.* **2020**, *11*, 1–13; c) X. Zhang, N. Wang, Y. Huang, Y. Li, G. Li, Y. Lin, A. J. Atala, J. Hou, W. Zhao, *The International Journal of Artificial Organs* **2022**, *45*, 181–192.

[24] a) R. Toghiani, V. Azimian Zavareh, H. Najafi, M. Mirian, N. Azarpira, S. S. Abolmaali, J. Varshosaz, A. M. Tamaddon, *Stem Cell Res. Ther.* **2024**, *15*, 240; b) S. Sart, A.-C. Tsai, Y. Li, T. Ma, *Tissue Eng., Part B* **2014**, *20*, 365–380.

[25] a) P. Kumar, S. Ciftci, J. Barthes, H. Knopf-Marques, C. B. Muller, C. Debry, N. E. Vrana, A. M. Ghaemmaghami, *J. Tissue Eng. Regener. Med.* **2020**, *14*, 45–57; b) Y. Xue, H. J. Kim, J. Lee, Y. Liu, T. Hoffman, Y. Chen, X. Zhou, W. Sun, S. Zhang, H.-J. Cho, J. Y. Lee, H. Kang, W. H. Ryu, C.-M. Lee, S. Ahadian, M. R. Dokmeci, B. Lei, K. Lee, A. Khademhosseini, *Small* **2022**, *18*, 2107714; c) D. W. Nelson R. J. Gilbert, *Adv. Healthcare Mater.* **2021**, *10*, 2101329; d) K. Hayashi Y. Tabata, *Acta Biomater.* **2011**, *7*, 2797–2803; e) L. Ferroni, C. Gardin, U. D'Amora, L. Calzà, A. Ronca, E. Tremoli, L. Ambrosio, B. Zavan, *Biomater. Adv.* **2022**, *139*, 213000.

[26] a) M. E. Ogle, G. Doron, M. J. Levy, J. S. Temenoff, *Tissue Eng., Part A* **2020**, *26*, 1259–1271; b) R. Olivares-Navarrete, E. M. Lee, K. Smith, S. L. Hyzy, M. Doroudi, J. K. Williams, K. Gall, B. D. Boyan, Z. Schwartz, *PloS One* **2017**, *12*, e0170312; c) M. Sun, G. Chi, J. Xu, Y. Tan, J. Xu, S. Lv, Z. Xu, Y. Xia, L. Li, Y. li, *Stem Cell Res. Ther.* **2018**, *9*, 1–13.

[27] S. Jeon, J. H. Heo, M. K. Kim, W. Jeong, H. W. Kang, *Adv. Funct. Mater.* **2020**, *30*, 2005324.

[28] a) R. Somadder, L. Faraj, S. Datta, M. Kanapathipillai, G. Ghosh, *Biotechnol. J.* **2024**, *19*, 2300474; b) Y. Huang, X. Li, L. Yang, *Frontiers in Bioengineering and Biotechnology* **2022**, *10*, 859927.

[29] a) H. Brem, M. S. Golinko, O. Stojadinovic, A. Kodra, R. F. Diegelmann, S. Vukelic, H. Entero, D. L. Coppock, M. Tomic-Canic, *J. Transl. Med.* **2008**, *6*, 1–9; b) I. B. Wall, R. Moseley, D. M. Baird, D. Kipling, P. Giles, I. Laffafian, P. E. Price, D. W. Thomas, P. Stephens, *J. Invest. Dermatol.* **2008**, *128*, 2526–2540.

[30] a) A. Shabbir, A. Cox, L. Rodriguez-Menocal, M. Salgado, E. V. Badiavas, *Stem Cells Dev.* **2015**, *24*, 1635–1647; b) L. Hu, J. Wang, X. Zhou, Z. Xiong, J. Zhao, R. Yu, F. Huang, H. Zhang, L. Chen, *Sci. Rep.* **2016**, *6*, 32993.

[31] a) Y. Zhang, M. Chopp, Z. G. Zhang, M. Katakowski, H. Xin, C. Qu, M. Ali, A. Mahmood, Y. Xiong, *Neurochem. Int.* **2017**, *111*, 69–81; b) T. Zhang, H. Chen, Y. Zhang, Y. Zan, T. Ni, M. Liu, R. Pei, *New J. Chem.* **2019**, *43*, 1980–1986.

